Oil Spills Detection: Challenges addressed in the scope of the SEAGULL project

Mario Monteiro Marques & Vitor Lobo
Centro de Investigação Naval (CINAV)
Marinha de Guerra Portuguesa (MGP)
Almada, Portugal

Maria de Fátima Nunes
Centro de Investigação da Academia da Força Aérea
Força Aérea Portuguesa (FAP)
Sintra, Portugal

Ricardo Batista & J. Almeida
Critical Software, S.A.
Lisboa, Portugal

Ricardo Ribeiro & Alexandre Bernardino
Instituto de Sistemas e Robótica (ISR)
Instituto Superior Técnico (IST)
Lisboa, Portugal

Abstract –The development of intelligent systems to support maritime situation awareness is the main goal of the SEAGULL project. By equipping unmanned aerial vehicles (UAVs) with different types of optical sensors we target an intelligent maritime surveillance system. In this paper we present experiments performed with an hyperspectral camera to detect oil spills. We have developed a detection algorithm that automatically informs the base station of an oil spill in case a spectral signature recognized as oil is found on open sea. This contributes significantly to the generation of situational awareness of maritime events such as detection and georeferencing of oil spills or hazardous and noxious substances. After a brief overview of the SEAGULL platform and architecture, we focus on presenting the algorithms for automatic detection of oil spills with a hyperspectral camera on board an UAV.

Keywords—Computer Vision; Unmanned Aerial Vehicles; Oil Spills.

I. INTRODUCTION

In the world, around 90,000 thousand barrels of oil are consumed each day and about 80% of these barrels are transported by ship. The International Tanker Owners Pollution Federation Limited (ITOPF) categorises the oil spills by size – less than 7 tonnes; between 7 tonnes and 700 tonnes; and more than 700 tonnes. Since 1967, more than 10000 accidents have been registered and from these, 81% rank in the less than 7 tonnes categories. Of the 20 major oil spills, 19 occurred before 2000 [1]. Two large spills (>700 tonnes) were recorded on 2015. Both releases of oil occurred as a result of a collision. The first, in Singapore in January, resulted in a spill of approximately 4,500 tonnes of crude oil and the second, in Turkey in June, resulted in a spill of approximately 1,400 tonnes of naphtha.

Optical sensors such as cameras (visible, infrared, multi- and hyper spectral) can contribute significantly to the generation of situational maritime awareness, and particularly in environmental protection like the detection of maritime oil spills.

The SEAGULL project proposes to create an intelligent maritime surveillance system by equipping Unmanned Autonomous Vehicles (UAVs) with such different types of optical sensors.

In this scenario, the use of unmanned autonomous vehicles, particularly aircrafts with high autonomy, intelligence and reduced needs of communication and human resources, appears as a very promising, perhaps unavoidable, alternative. With all the existing maritime area to monitor, the validation of one more asset to conclude such tasks is primordial.

Therefore, the project aims to develop efficient solutions to address the challenges of maritime situational knowledge management. This perception is essential in maritime operations related to the safety of life at sea, security and environmental protection.

This paper is organized as follows. In Section II the architecture of the SEAGULL project's platform is described. Section III shows the preliminary tests realized and the results obtained. Based on these, Section IV explains how the automatic detection of oil spills is performed and shows the results obtained using it. In section V are given some conclusions on the matter.

II. SEAGULL PLATFORM ARCHITECTURE

The SEAGULL system is comprised by: *(i)* the UAV microcontroller autopilot and respective ground station for navigation control and telemetry; *(ii)* the onboard command and control computer to support communication and navigation-specific functionalities; *(iii)* the payload sub-systems (secondary onboard computer and ground station), and *(iv)* the onboard sensors coupled with the UAV to perform image detection and auxiliary functionalities.

978-1-5090-1537-5/16/$31.00 ©2016 IEEE

Figure 1: Tests of SEAGULL UAV platform

The system used in the SEAGULL project is based in Commercial of the shelf (COTS) components. The major driver for this decision was the capability to be independent of specific manufacturers and the capability to easily exchange different modules in the platform.

The usage of COTS components in the UAV allows two different goals: (1) maintain the total cost of the platform at a very low level, and (2) enable the system modularity with the usage of different sensors from several manufacturers.

The SEAGULL platform was based in the UAV platform shown in Figure 1 and the ground segment composed by two stations. The physical architecture is presented in Figure 2.

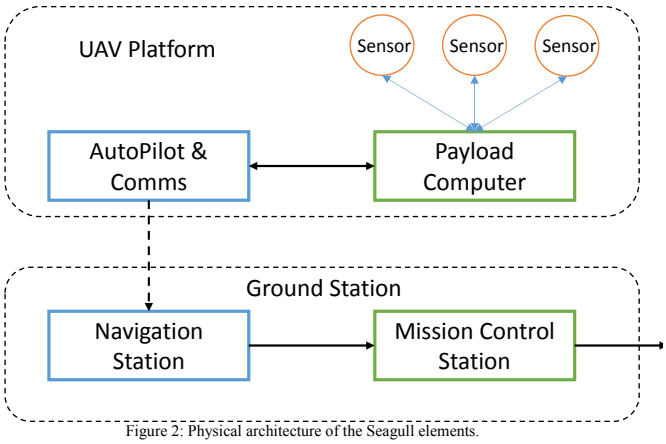

Figure 2: Physical architecture of the Seagull elements.

The UAV platform is composed by a computer with the COTS autopilot and communication equipment. This computer is responsible for the UAV navigation capabilities. Associated with this computer is a DGPS sensor that provides accurate positions to the autopilot system.

III. Preliminary Tests and Results

The UAVs used in the Seagull project for flying tests were developed and manufactured at the Portuguese Air Force Research Center. This Center is focused on developing UAV technology and operational know-how for use in the context of maritime situational awareness (MSA), where it has accumulated long experience (about 1000 autonomous flights, adding up about 600 hours of flight), flying from several places along Portugal, such as Santa-Cruz airfield (located at Portuguese western coast), Portimão airfield (located at Portuguese south cost) and airport of Porto Santo (Portuguese Atlantic Island).

From the components that are part of the system's architecture, one particular sensor was selected with the specific purpose of detecting oil spills – a hyper-spectral camera designed for UAV usage.

Figure 3: Rikola hyper-spectral camera

The hyper-spectral camera is produced by Rikola (Figure 3) and presents several capabilities. The camera is sensitive to the visible and the near infra-red frequency bands and can acquire a full image frame for a given frequency in a single time instance. Multiple frequencies are swept in time. This needs to be taken into account because, due to the UAV motion, the images obtained for different frequencies are misaligned.

The camera has the ability to be pre-programmed to automatically record data into a memory card. This is particularly convenient when used with UAV's because no user interaction is necessary and no remote control communication channel is required. In this case, up to 25 pre-programmed frequency bands can be acquired using a frame rate up to one full spectrum image per each two seconds.

However, due to the inner complexity of the camera, the sweep of the frequencies is not monotonic as shown in Figure 4.

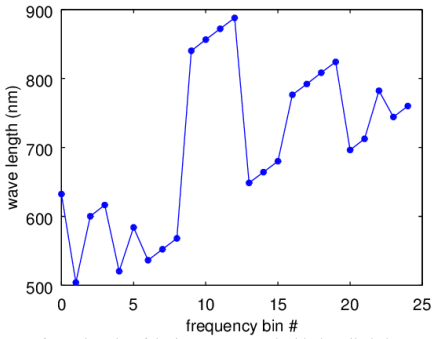

Figure 4: Sequence of wavelengths of the images captured with the Rikola hyper-spectral camera. The images are acquired by the order of the frequency bin number.

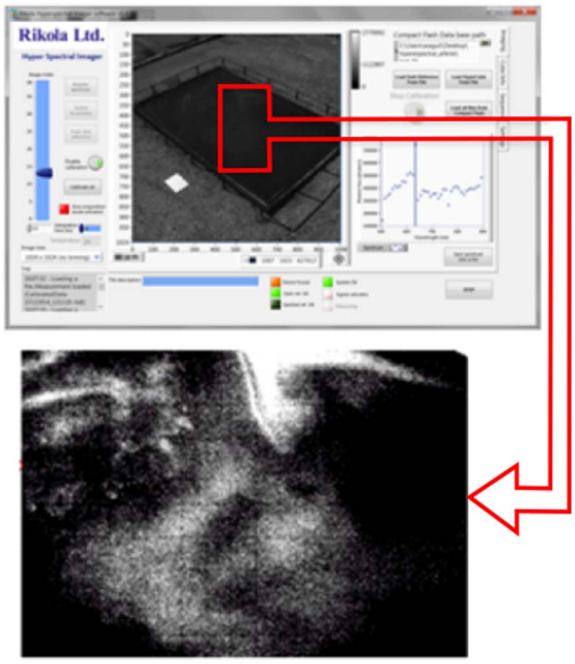

Figure 5: Hyper-spectral camera usage in laboratory tests (fish oil spills in tank)

For the hyper-spectral camera tests, two types of environments were used. Laboratory tests (Figure 5) were performed in the Portuguese Navy laboratories, consisting of camera usage to record oil spills in water tanks. The results provided the necessary data to understand the camera's capabilities and design an algorithm capable of collecting the images and performing computations to detect oil patterns. Field tests (Figure 6) were performed in the ocean, consisting of camera usage aboard the UAV, flying over the ocean and recording images of fish-oil spills dropped to the sea by a fast patrol boat from the Portuguese Navy (about 100 litters spilled in front of the lighthouse of Ponta da Piedade – Lagos about 4 miles from coast). The fish-oil was selected between several candidates, since it presented the closest pattern to the regular boat oil spills and its usage did not pose any particular risk to the environment.

The analysis of hyperspectral images captured in laboratory revealed that the spectrum of the image is different for the oil spill when compared to the spectrum of the unpolluted water. We can see in Figure 5 an example where oil was spilled into a tank of water. The oil is immediately recognizable if we look at specific frequencies of the acquired spectrum.

The same type of difference in the spectrum is observed in the field tests, however, due to the UAV motion, the images for different frequencies are not aligned (Figure 6) and it is difficult to obtain the full spectrum corresponding to a single point in the sea.

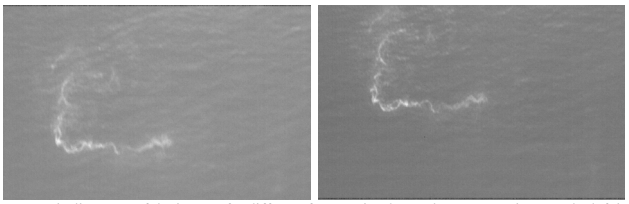

Figure 6: Misalignment of the images for different frequencies due to the UAV motion. On the left is the image for frequency #0 (632.4 nm) and on the right for frequency #15 (680 nm). The luminance of the images was increased in order for the pollutant to be seen.

Figure 7 compares two spectral plots obtained for two different points, one containing pollutants and the other with clean sea. Due to the UAV motion, only the lower frequency bins are a reliable representation of the spectrum, since the upper frequency bins no longer correspond to a point in the sea in the same region as the lower bins due to the misalignment of the images.

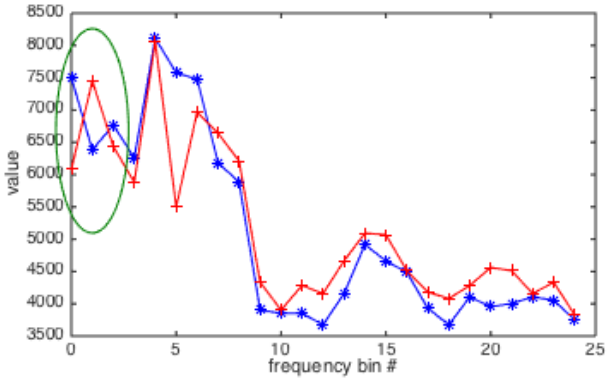

Figure 7 – Spectrum plots for polluted sea (*, blue color) and for normal sea (+, red color). Inside the green circle are the points to be used by the detection algorithm.

Nevertheless, we can observe that the first three bins (marked by the green circle in Figure 7) contain enough information to distinguish between polluted and unpolluted sea. Notice how the value for bin #1 is smaller than for bins #0 and #2 when there is pollution, and larger otherwise. This characteristic behaviour is also confirmed by the data obtained at the laboratory tests.

Notice in Figure 4 that bin #1's wavelength (504.1 nm) is very different of the wavelengths of bins #0 and #2 (632.4 nm and 600.2 nm, respectively). Due to the non monotonic ordering of the frequencies, they end up being close together. This also implies that the misalignment between them, even though present, will not be excessively large.

The detection algorithm we will present bellow will try to benefit from these characteristics to mark the sea areas that are polluted while avoiding the difficult task of aligning the images.

IV. AUTOMATIC DETECTION OF OIL SPILLS

Since there is misalignment of the images for different spectral bands, state of the art methods to analyse the hyperspectral content, such as spectral signature matching [2] or end-member extraction methods [3] cannot be applied in a straightforward manner. We propose a new method based on simple logic rules and on morphological transforms based on the erosion and dilation operators [4]. The new method is able

to successfully detect oil spills and is robust to the misalignment of the images.

A. Rule based detection

The detection is going to be based on the comparison of the relative values of the three frequency components s_0 (632.4 nm), s_1(504.1 nm) and s_2(600.2 nm). The basic idea is to test if band s_1 has a larger amplitude than both s_0 and s_2 This is coherent with the study of Zhao and Cong [5] that showed that oil spills offshore have peaks in the spectral region from 500nm to 580nm.

Because we are interested in the relative amplitude between different bands (the absolute value is only dependent on the overall luminance), the first step is to normalize the components so that

$$\left|\left|(s_0, s_1, s_2)^T\right|\right|_2 = \sqrt{s_0^2 + s_1^2 + s_2^2} = 1$$

where $(s_0, s_1, s_2)^T$ is a column vector containing the three components and $\left|\left|\ \right|\right|_2$ represents the two-norm of the vector.

After normalization, the values of the normalized spectrum components are compared. Specifically, s_0 and s_2 are compared to s_1 and two masks result from this comparison

$$mask01 = (s_1 > s_0)\ \&\ !\,Mask_Y$$
$$mask12 = (s_1 > s_2)\ \&\ !\,Mask_Y,$$

where $Mask_Y$ is a luminance mask to avoid bright objects (e.g. boats, see next subsection), & is the logic and operator and ! is the logic negation.

These masks are first eroded with a 3 by 3 pixels disk and then dilated by a 31 by 31 pixels disk.

$$Mask01 = dilate\ (\ erode\ (\ mask01\ ))$$
$$Mask12 = dilate\ (\ erode\ (\ mask12\ ))$$

See example in Figure 8.

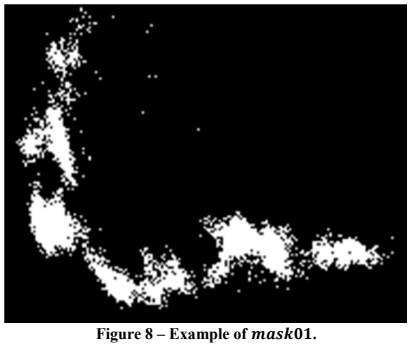

Figure 8 – Example of *mask*01.

The erosion eliminates random isolated points (Figure 9) that appear throughout the whole image due to the camera's sensor noise. Larger sets of points on the masks, that correspond to polluted areas, are slightly reduced in size by the erosion but aren't eliminated. The dilation that follows will regrow those areas (Figure 10).

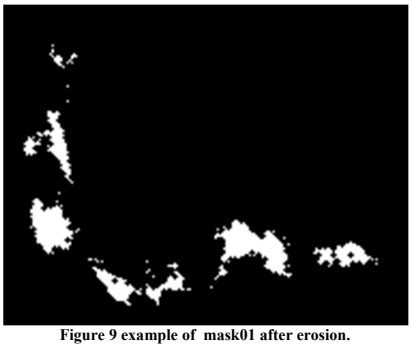

Figure 9 example of mask01 after erosion.

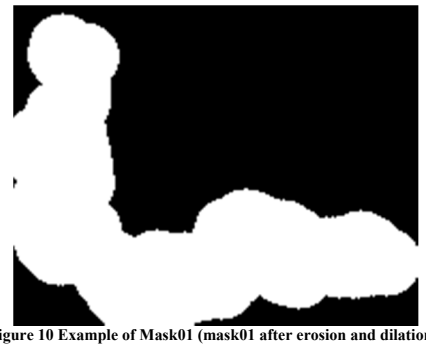

Figure 10 Example of Mask01 (mask01 after erosion and dilation).

The dilation kernel was chosen large enough so that the positive areas of the masks will overlap in spite of the misalignment of the images (Figure 11). The detection mask is the intersection of both masks

$$mask_{detection} = Mask01\ \&\ Mask12$$

and is also dilated with a 15 by 15 pixels disk to remove small gaps and to enlarge it a bit further.

$$Mask_{detection} = dilate(\ mask_{detection}\ )$$

See in Figure 12 the final result of the detection.

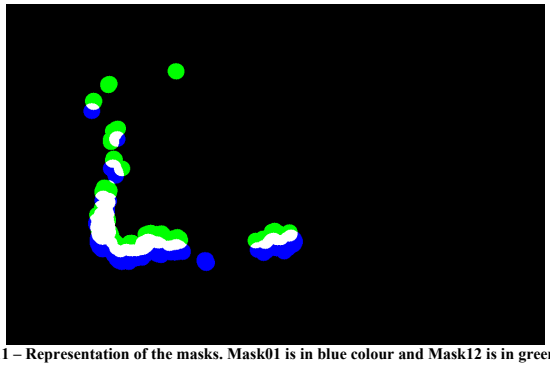

Figure 11 – Representation of the masks. Mask01 is in blue colour and Mask12 is in green colour. The areas in white color are common to both masks.

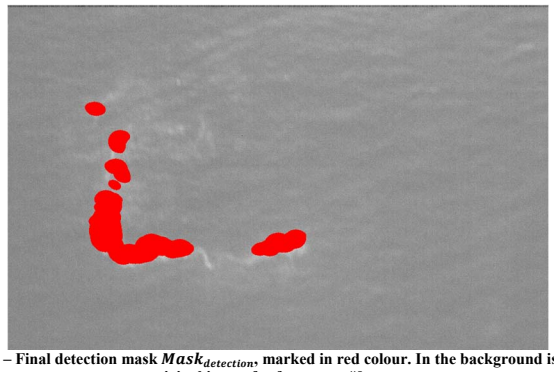

Figure 12 – Final detection mask $Mask_{detection}$, marked in red colour. In the background is the original image for frequency #0.

B. *Other objects*

Besides pollutants, there are other objects on the sea, like the boat shown in Figure 13. These objects are well illuminated either directly by the sun or by diffuse light from the sky and are much brighter than the pollutant spills. Since we are solely interested in the pollutants, we need to make sure that these objects do not show up as false detections.

Figure 13 – An image containing a boat. There is also a pollutant spill (similar to the one in Figure 6) on the right side of the image that cannot be seen because the boat luminance is much larger. The pollutant is so dark compared to the boat that becomes indistinguishable from the background.

This is done applying a threshold to all the frequencies being analyzed and discarding all points for which at least one of them exceeds the threshold value. So we create a luminance mask $mask_Y$ such as

$$mask_Y = \left(s_0 > th_y\right) or \left(s_1 > th_y\right) or \left(s_2 > th_y\right),$$

where th_y is the luminance threshold value, and s_0, s_1 and s_2 are the spectral components for frequencies bins #0, #1 and #2, respectively.

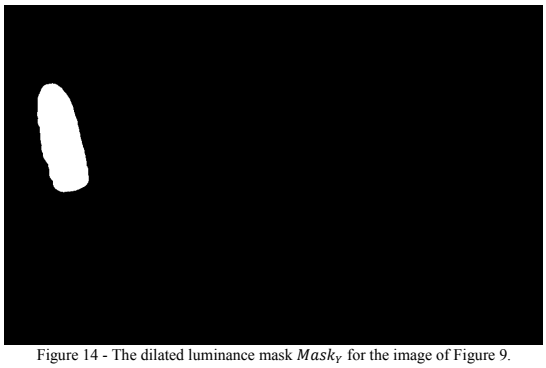

Figure 14 - The dilated luminance mask $Mask_Y$ for the image of Figure 9.

This mask is then enlarged by a dilation operation using a 29 by 29 pixels round kernel (see Figure 14). This amount of enlargement provides a safety area sufficiently large to account for any misalignment between frequencies. The dilated luminance mask

$$Mask_Y = dilate(mask_Y)$$

will be used on the remaining of the detection algorithm as shown in the previous subsection and the result is shown in Figure 15.

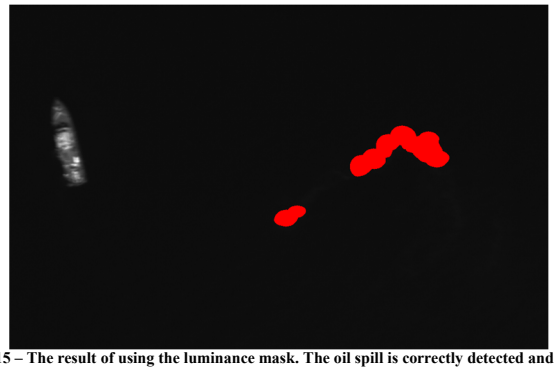

Figura 15 – The result of using the luminance mask. The oil spill is correctly detected and the boat is ignored.

C. *Detection Results*

This algorithm is successful in the detection of fish oil pollutant spills as is show in several example images depicted in Figure 12 and in Figure 16. Also, Figures 15 and 17 show that the algorithm is insensitive to the presence of boats on the image, marking only the oil spills and not the boats.

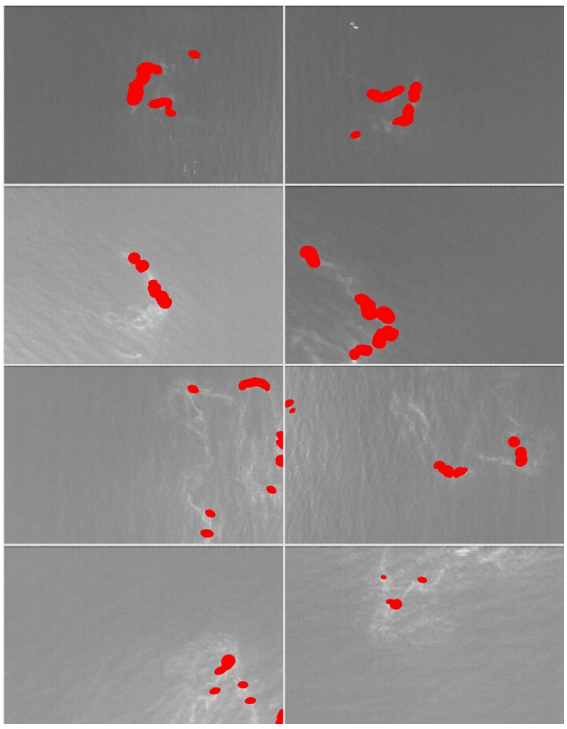

Figure 16 - Detections (marked in red color) obtained for several example image frames. The brightness of the images was increased in order for the oil spills to be clearly visible.

Figure 17 - Detection examples for some image frames containing boats.

V. Conclusions

The main goal of this work was the development of a system that can be attached to UAV's and detect, identify and track oil spills at sea. After several tests, real and simulated, the developed algorithm has successfully fulfilled the proposed objectives.

The work of this project has shown the viability of the use of UAV's equipped with hyperspectral cameras for the purpose of detecting pollutants in the sea in an automatic way. Also, as a result of this work, a new database containing a valuable number of hyper-spectral images of pollutants in the sea is now available for future research.

Analysis of the hyperspectral images obtained by the onboard camera reveal that oil and sea water have different spectral signatures. However, due to UAV motion, different frequency bands are misaligned, which prevents a straightforward application of common spectral signature detection algorithms. Thus, a new rule based method is proposed to detect oil spills. This new method is robust to the misalignment between the images and is also robust to the presence of other object like boats. Results show that when applying the new method to the captured data, the oil spills are correctly identified.

Acknowledgment

This work was funded by POFC (Programa Operacional Factores de Competitividade) within the National Strategic Reference Framework (QREN) under grant agreement 2013/034063(SEAGULL, project number 34063), and by the national science foundation (FCT) through project UID/EEA/50009/2013.

References

[1] Mario Monteiro Marques, P. Dias, N. Santos, V. Lobo, R. Batista, D. Salgueiro, R. Ribeiro, J. Marques, A. Bernardino, M. Griné, M. Taiana, M. Nunes, E. Pereira, J. Morgado, A. Aguiar, M. Costa, J. Silva, A. Ferreira, J. Sousa, "Unmanned Aircraft Systems in Maritime Operations: Challenges addressed in the scope of the SEAGULL project," in MTS/IEEE OCEANS 2015, 2015, pp. 1–6.

[2] Mohammad S. Alam and Paheding Sidike. Trends in oil spill detection via hyperspectral imaging. Institute of Electrical and Electronics Engineers, pages 858–862, December 2012. ISBN:978-1-4673-1436-7.

[3] Dimitris Sykas, Vassilia Karathanassi, Charoula Andreou, and Polychronis Kolokoussis. Oil spill mapping using hyperspectral methods and techniques. Automatic Oil-Spill Recognition and Geopositioning integrated in a Marine Monitoring Network (ARGOMARINE) , 2012

[4] David Forsyth, Jean Ponce – "Computer Vision: A Modern Approach", Pearson, 2012

[5] D. Z. Zhao and P F. Cong. The research of visual light wave-band feature spectrum. In Remote Sens. Technology, volume 15(3), pages 160–164. 2000.